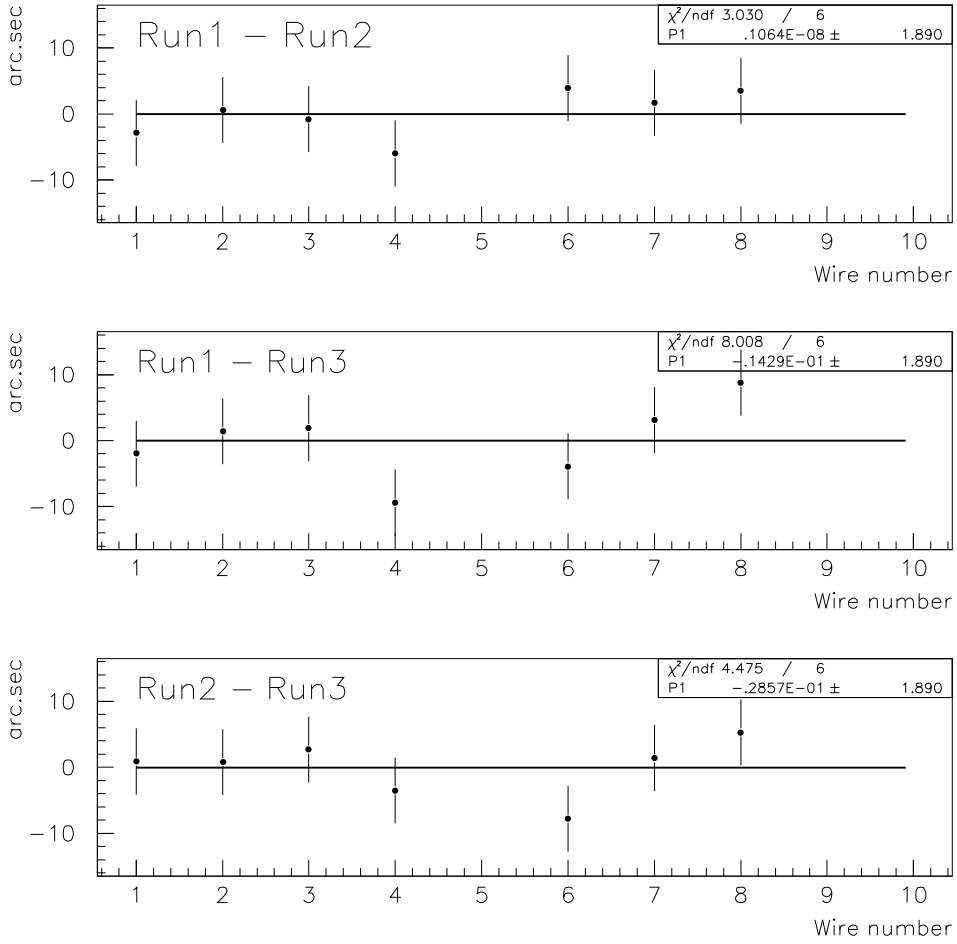

Figure 17: For seven wires of the calibration wheel, difference between the measurements of their angular position φ at various points in time.

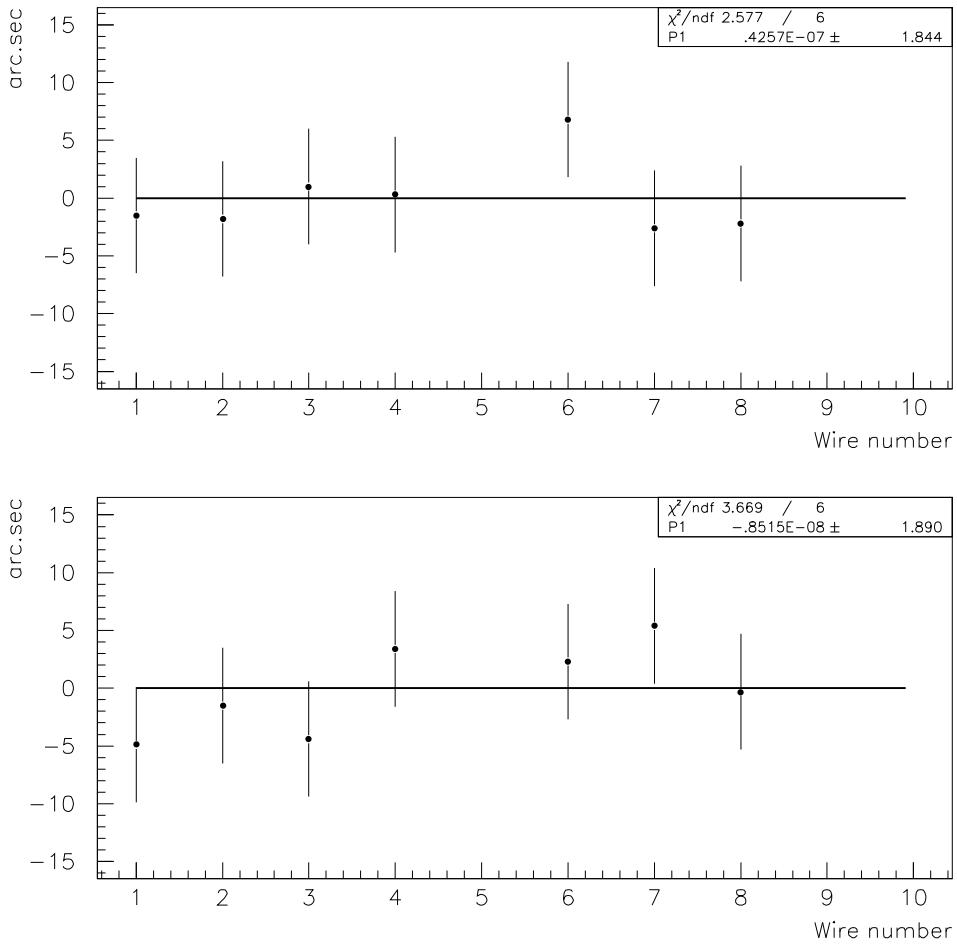

Figure 16: For seven wires of the calibration wheel, difference between the two metrology measurements of their angular position φ (top) and between the average values of the metrology and BDD measurements (bottom).

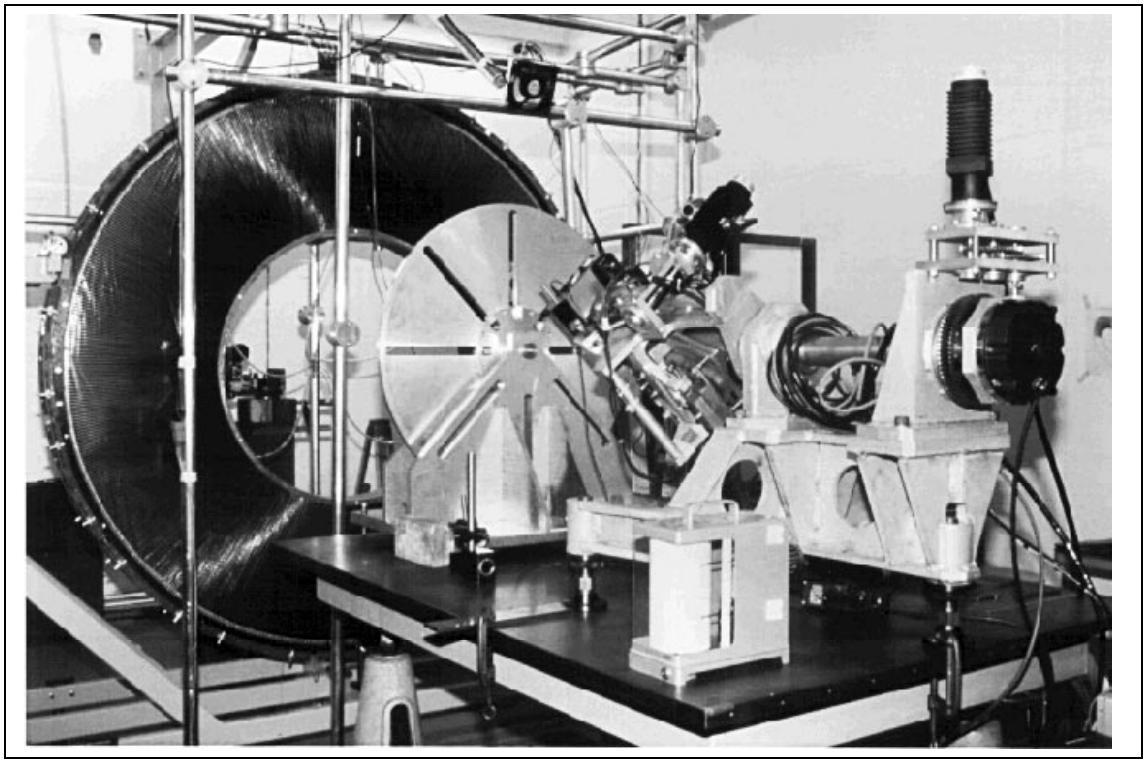

Figure 15: Photograph of the Beam Directing Device with the metallic calibration wheel installed on a rigid table in front of it. Behind this wheel , part of the prototype endcap TRT wheel is also visible

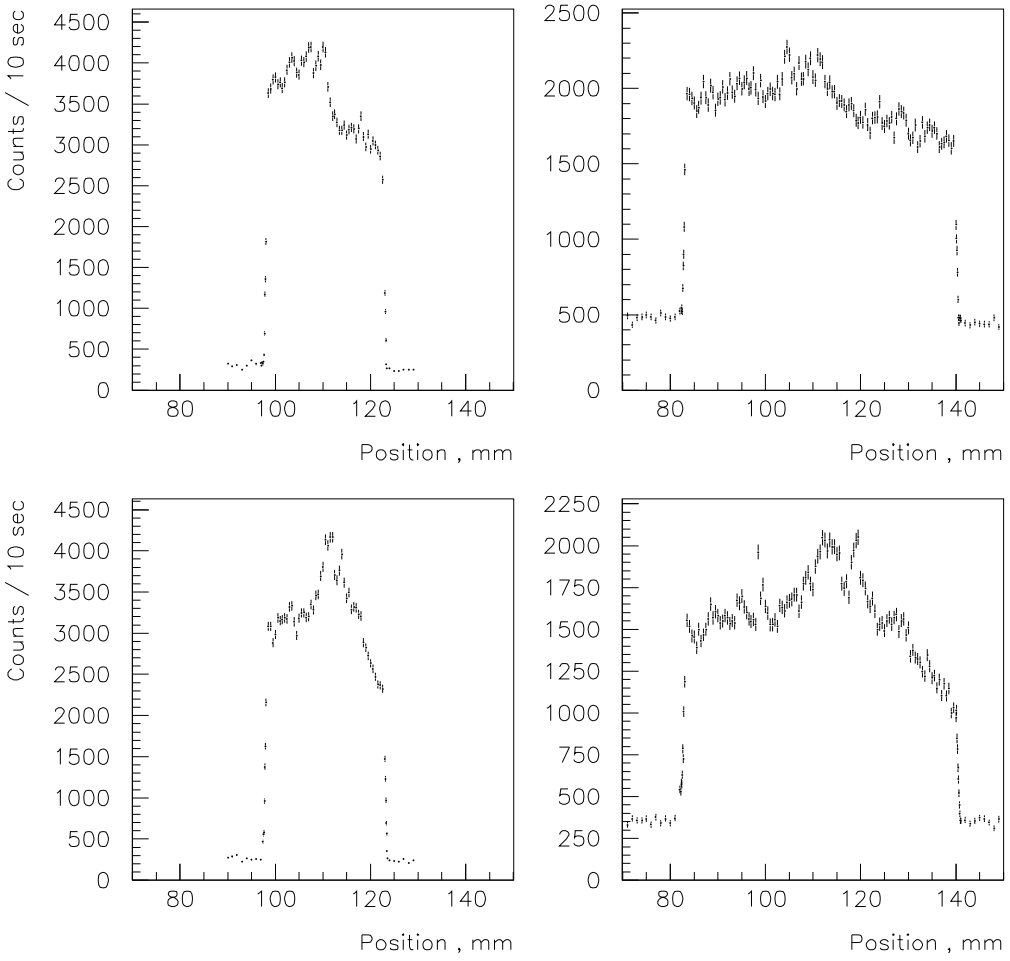

Figure 14: Profiles of the X-ray beam in the vertical direction (broad component of them). In this direction, the exit slit has a size of 22 mm. The left-hands plots correspond to a measurement close to the exit slit, and the right-hand plots to a measurements at a distance 500 mm from it. The top (respectively bottom) plots corresponds to the BDD position before (respectively after) rotation by 180^o around the g_φ axis.

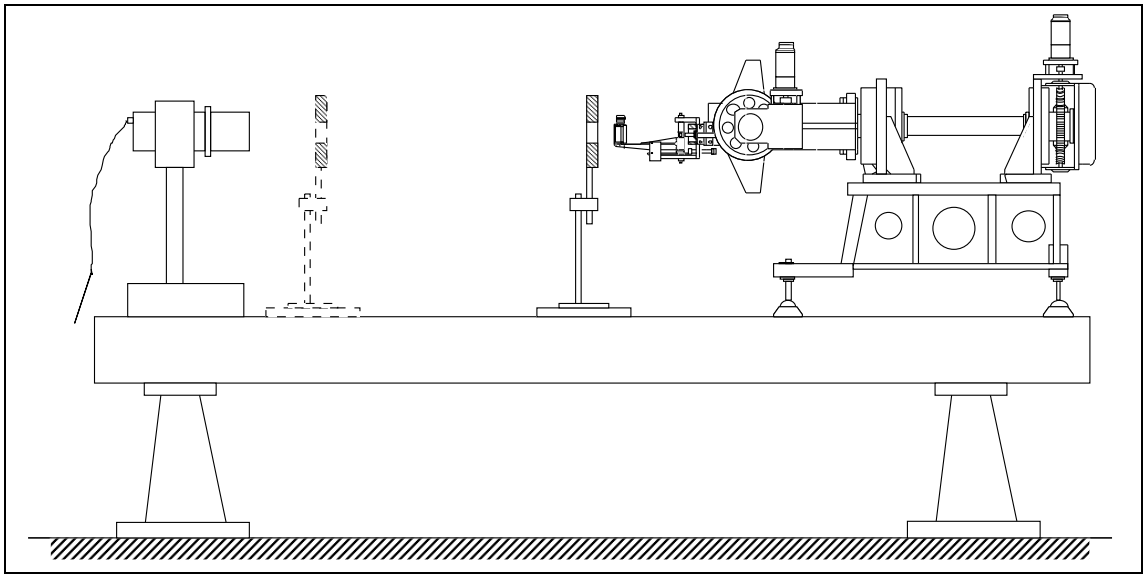

Figure 13: Sketch of the set-up for adjustment of the X-ray beam with respect to the g_φ axis in the vertical direction.

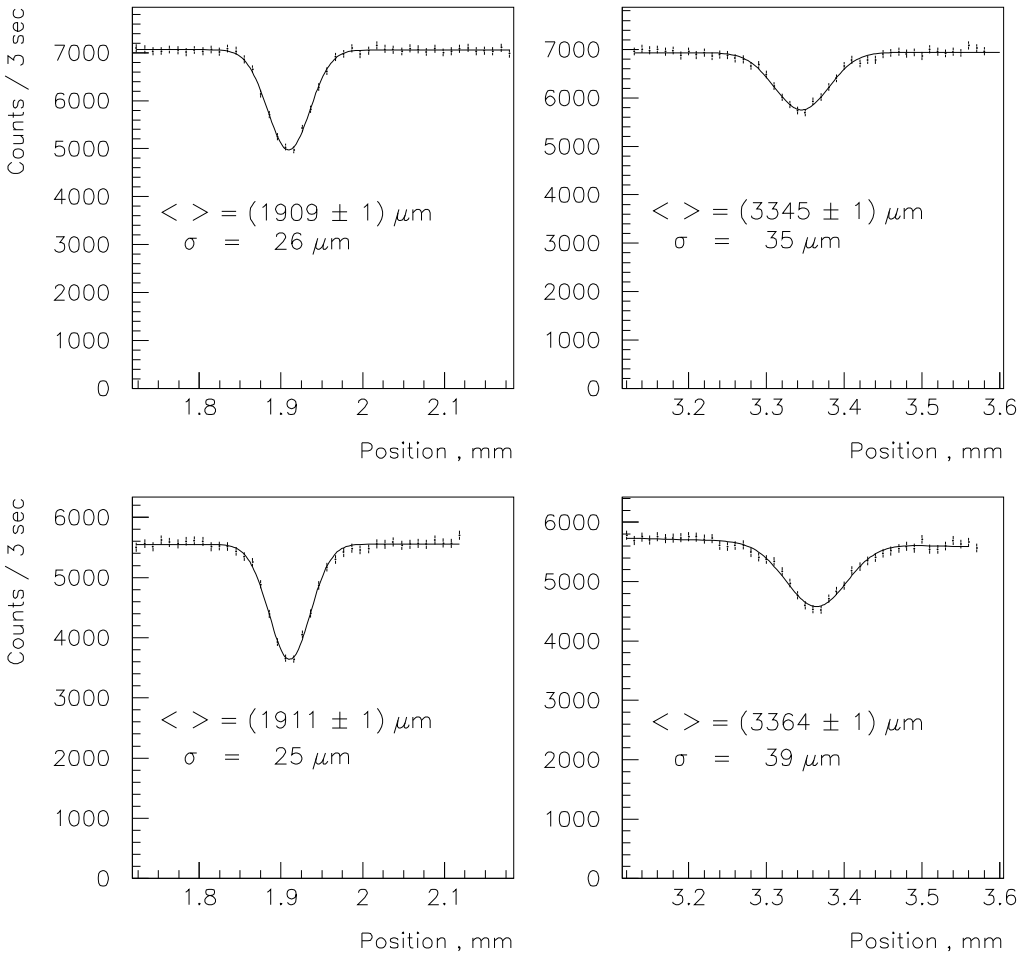

Figure 12: Shadow profiles from vertical tungsten wires placed in the path of the X-ray beam. The left-hand plots correspond to the wire placed close to the exit slit of the X-ray beam, and the right-hand plots to the wire placed at a distance of $\sim$ 500 mm. The top (respectively bottom) plots correspond to the BDD position before (respectively after) rotation by 180^o around the g_φ axis.

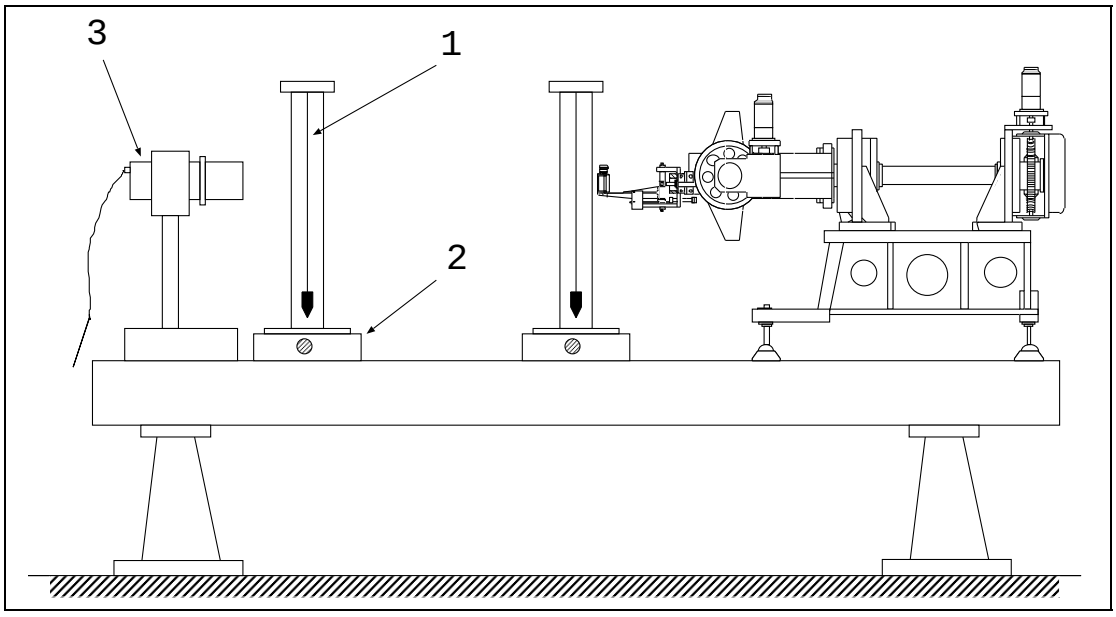

Figure 10: Sketch of the set-up for adjustment of the X-ray beam with respect to the g_φ axis in the horizontal direction.

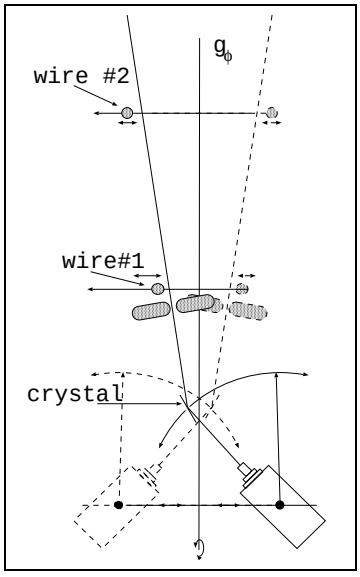

Figure 11: Illustration explaining the principle of the adjustment of the X-ray beam with respect to axis g_φ

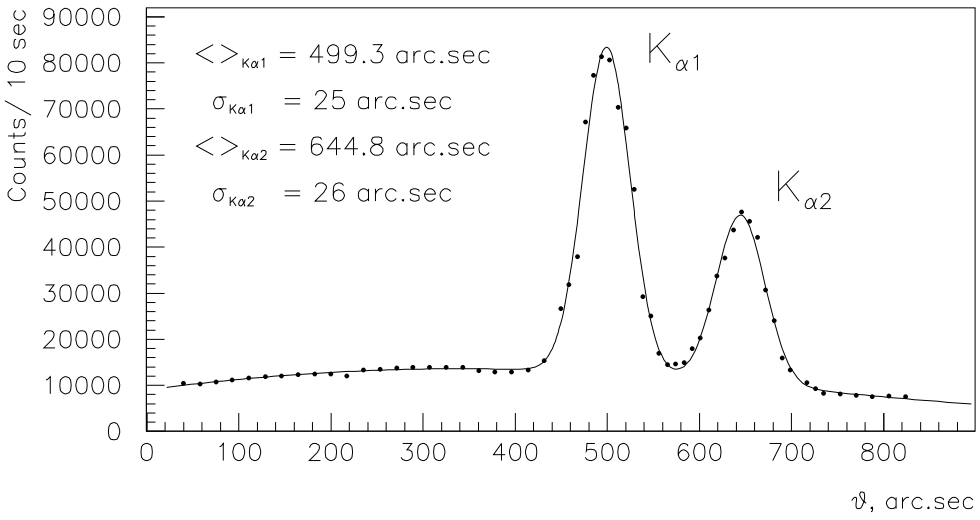

Figure 8: Counting rate after exit slit of X-ray monochromator as function of angle position of crystal ϑ.

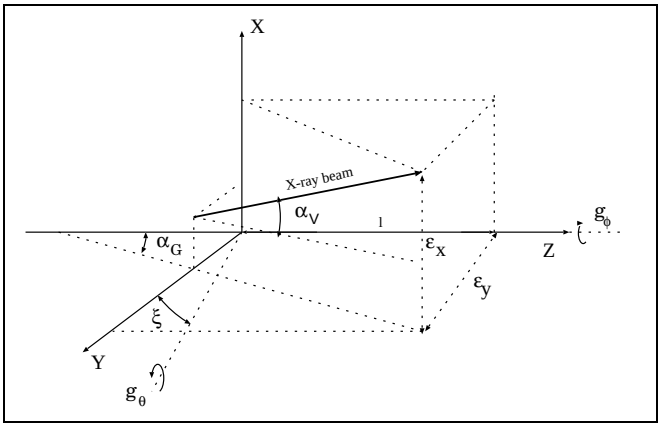

Figure 9: Coordinate systems used for BDD measurements.

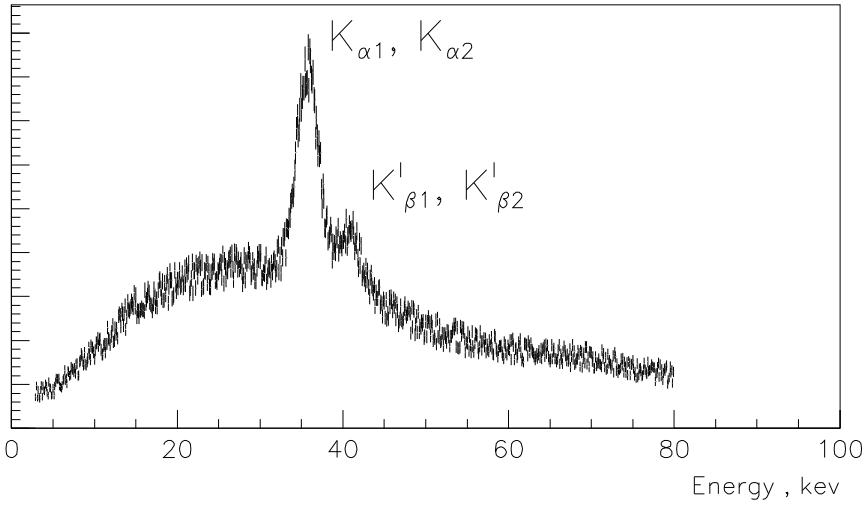

Figure 6: Energy spectrum of the produced X-ray beam, measured with a Ge(Li) detector in front of the monochromator.

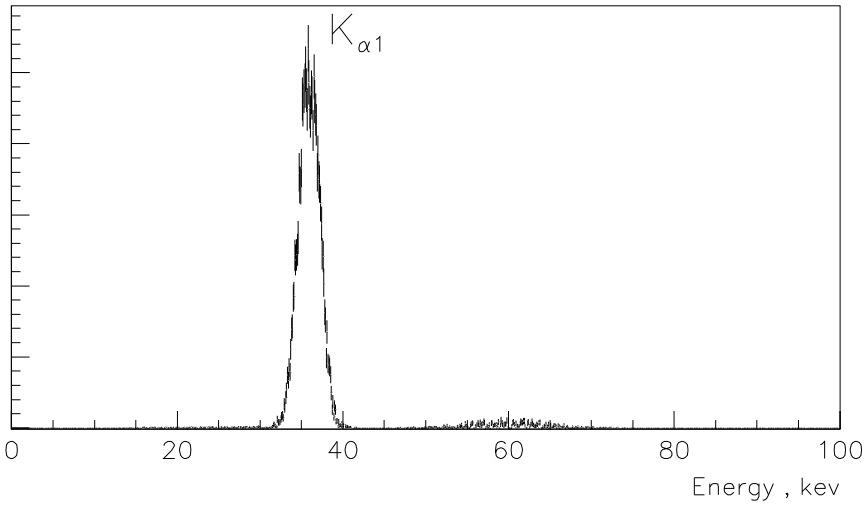

Figure 7: Energy spectrum of the X-ray beam, as measured behind the monochromator.

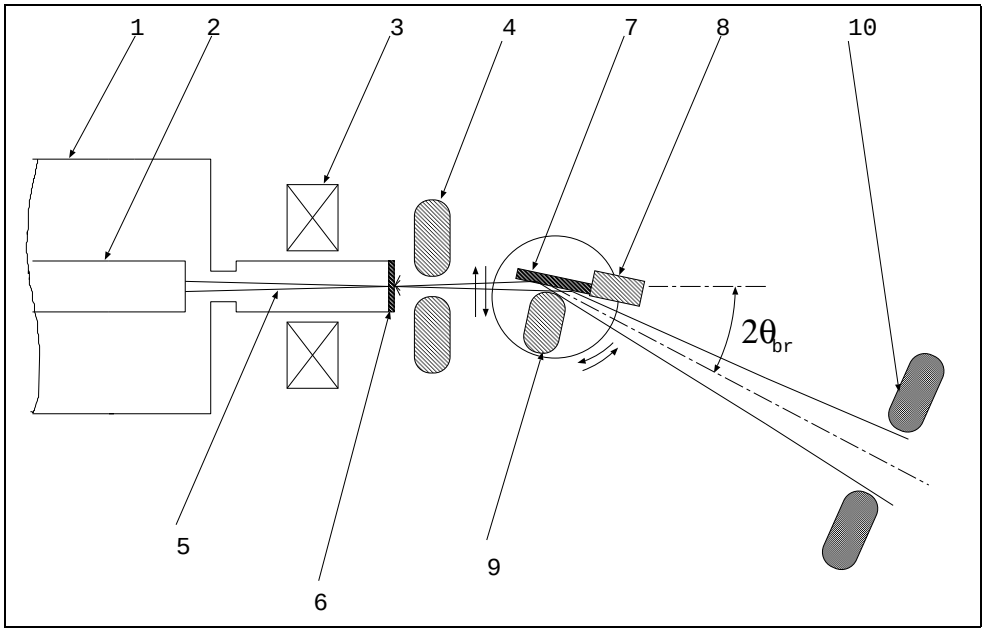

Figure 4: Sketch of the X-ray tube and the monochromator.

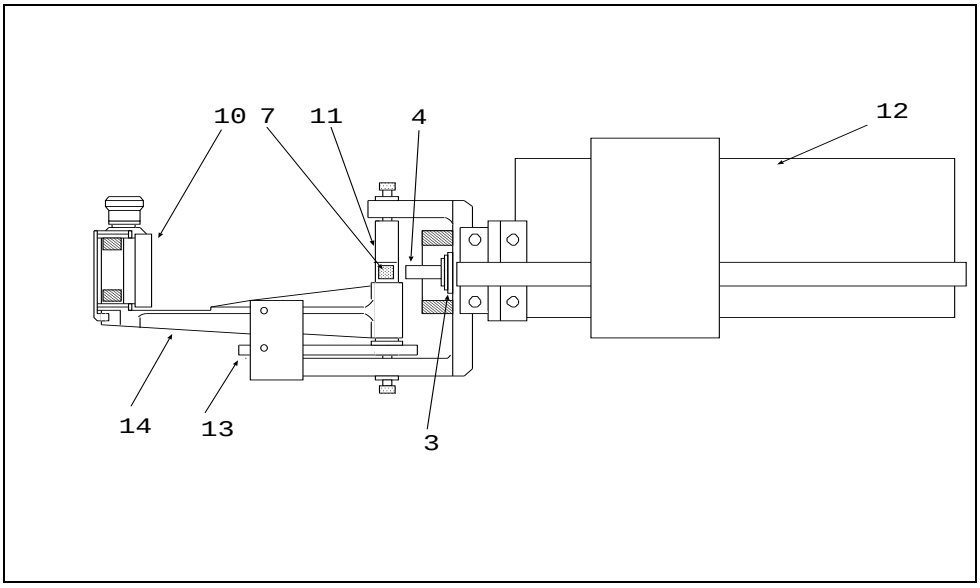

Figure 5: Design of the X-ray monochromator.

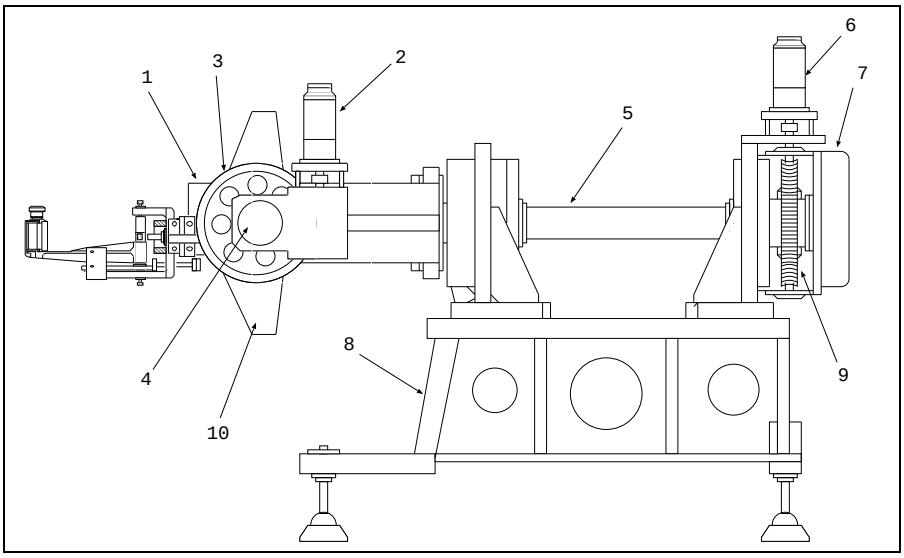

Figure 2: Schematic view of the Beam Directing Device

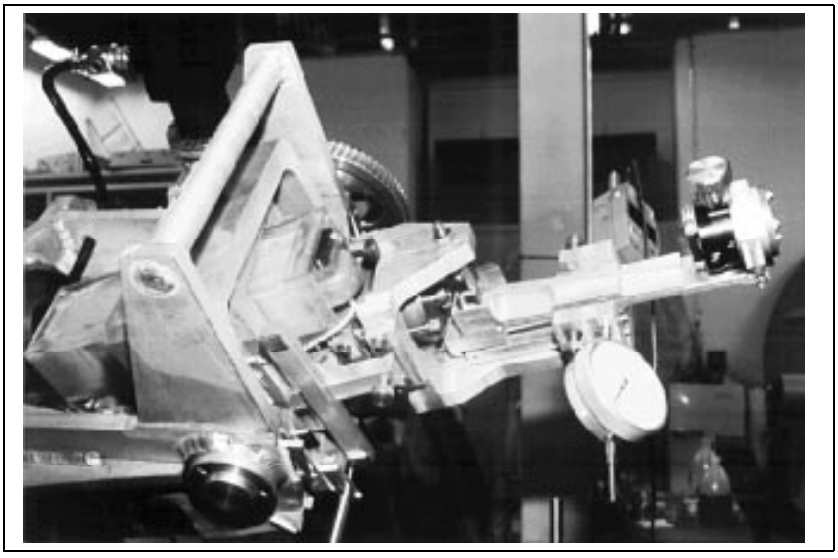

Figure 3: View of the X-Ray monochromator installed inside the moveable frame of the Beam Directing Device

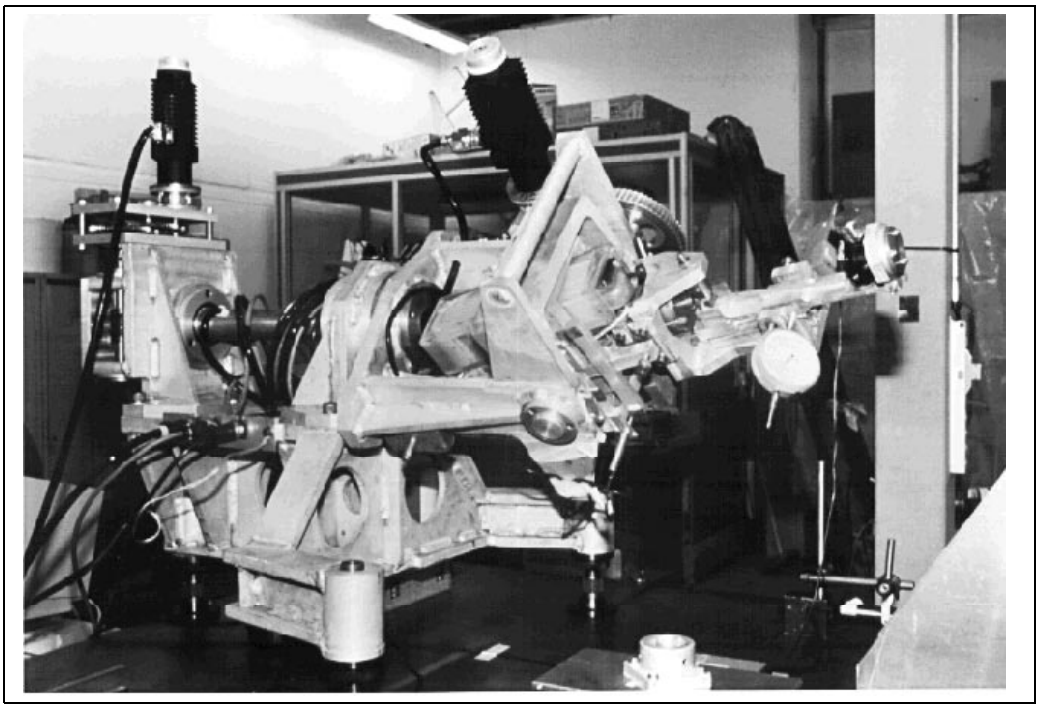

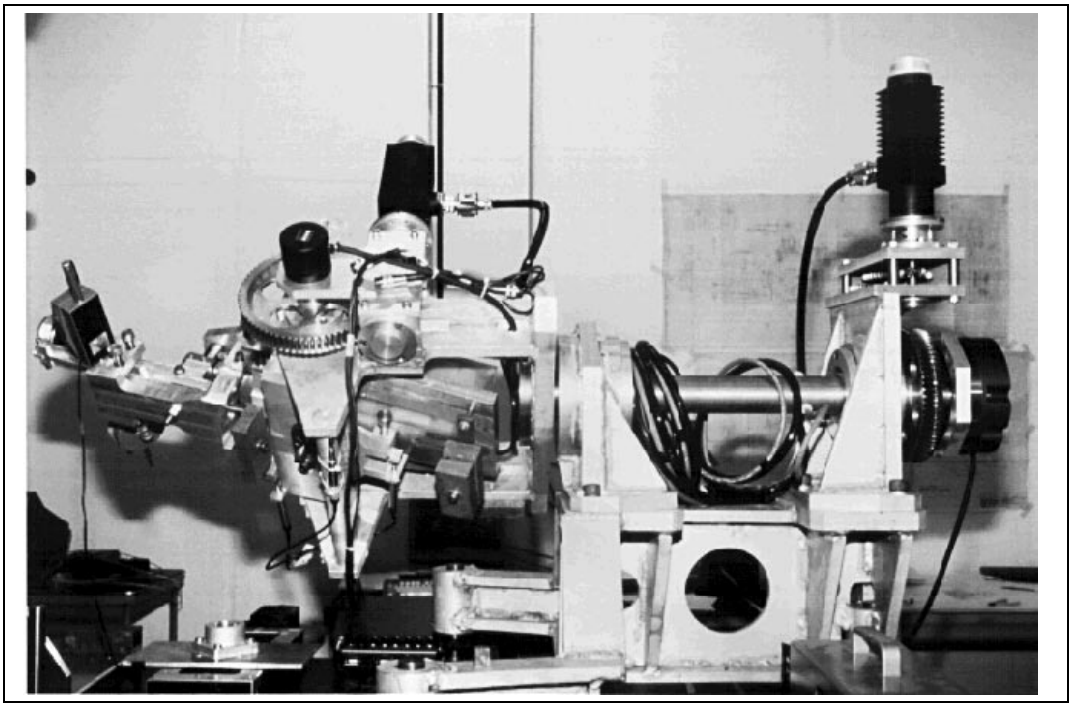

Figure 1: View of the Beam Directing Device from two sides.

List of Figures

References

[1] O. Fedin, A. Smirnov, On a possibility to use a narrow X-ray beam for straw proportional tube alignment, RD6 NOTE 51 (1994).

[2] O. Fedin, S. Muraviev, A. Smirnov, First results of a TRT cell prototype alignment test with a 36 KeV X-ray beam, ATLAS Internal Note, INDET-No-057 (1994).

[3] O. Fedin, S. Muraviev, Yu. Platonov A. Smirnov, An X-ray test station for ATLAS TRT calibration, ATLAS Internal Note, INDET-No-073 (1994).

[4] A. Vorobyov et.al., Mass production of the CSC's for the GEM Muon System: Technical Proposal, GEM-TN-93-366 (1993), Section 6, Global alignment.

[5] Table of Isotopes , by ed. C.M.Lederer and V.S.Shirley, 1978, New York.

8 Appendix A

$$\frac{x'^2}{A^2} - \frac{y'^2}{B^2} = 1,$$

where

$$\begin{aligned}
x' &= (x\cos\varphi + y\sin\varphi)\cos\gamma + (-x\sin\varphi + y\cos\varphi + \xi da)\sin\gamma \\
y' &= -(x\cos\varphi + y\sin\varphi)\sin\gamma + (-x\sin\varphi + y\cos\varphi + \xi da)\cos\gamma \\
a &= 1 - \frac{\varepsilon_y}{\xi d} + \frac{\alpha_G l}{\xi d} \\
\tan 2\gamma &= -\frac{2\frac{\varepsilon_x}{d}(\xi + \alpha_G)}{1 - \frac{\varepsilon_x^2}{d^2} + (\xi + \alpha_G)^2} \\
\frac{1}{A^2} &= -\frac{1}{2d^2(\xi + \alpha_G)^2}\left\{1 - \frac{\varepsilon_x^2}{d^2} - (\xi + \alpha_G)^2 - \sqrt{1 + \tan^2 2\gamma}\right\} \\
\frac{1}{B^2} &= \frac{1}{2d^2(\xi + \alpha_G)^2}\left\{1 - \frac{\varepsilon_x^2}{d^2} - (\xi + \alpha_G)^2 + \sqrt{1 + \tan^2 2\gamma}\right\}
\end{aligned}$$

9 Appendix B

$$x^2 + y^2 = d^2\left\{(\xi\frac{1 - \cos\vartheta}{\cos\vartheta} + \frac{\varepsilon_y}{d} + \alpha_G\frac{d - l\cos\vartheta}{d\cos\vartheta})^2 + (\tan\vartheta + \frac{\varepsilon_x}{d})^2\right\}$$

7 Acknowledgements

We gratefully acknowledge V.Schegelsky and D. Froidevaux for useful discussions. We thank K. Bussman, who has constructed the calibration wheel. We wish to express our gratitude to N. Dixon and all members from the TA1 group who helped us. We also wish to express our gratitude to C.Boudineau from the metrology service (MT/MF) for measuring the wire positions in the calibration wheel.

5.2 Results of the measurements

As mentioned above, the aim of the measurements was to compare the positions of the wires of the calibration wheel to the results obtained by the metrology service.

To check the mechanical stability of the wire positions and the reproducibility of the metrology results, the metrology service measurements were repeated after about one month (at the end of the calibration wheel measurements with the BDD). One of the eight wires (number 5) was excluded from the analysis due to an insecure inner fastening. The top plot of Fig.16 shows the differences between the two metrology measurements for the angular position Φ of each wire. The calculated value of the standard deviation between the two metrology results is σ=3.0″, corresponding to $\sim$ 15 μm at a distance of 1 meter.

The BDD measurements of the calibration wheel were performed three times of intervals of one week. The bottom plot of Fig.16 shows the differences between the average values of the angular position of each wire measured by the metrology and by the BDD. The calculated value of the standard deviation between the measurements is σ=3.6″. Finally Fig.17 shows the differences between the angular positions of each wire measured by the BDD at various points in time.

6 Conclusions

The experimental method and results described above have demonstrated that a high accuracy in the measurements of the endcap TRT wire positions can be achieved in φ, corresponding to $\sigma \leq 4''$ (or $\sim 20\mu$m at a distance of 1 m). It was also demonstrated, that distortions due to an imperfect coincidence of the X-ray beam direction with the Z axis do not deteriorate the accuracy of the measurements, because such distortions can be corrected for and the BDD can be adjusted to minimise their impact. Similarly, distortions arising because the exit slit of the monochromator is not perpendicular to the g_ϑ axis could be cancelled out by the measurement procedure itself. It should be noted, that in the latter case this doubles the time needed for the measurements.

A separate note describes the results of the measurements of the endcap TRT wheel prototype using the calibrated BDD.

from the wires was measured, using the NaI detector placed behind the wheel.

5.1 Measurement procedure

In the first approximation the wire projection in the XY plane is a straight line. The aim of the calibration measurements was extract the parameters of this straight line for each wire:

$$(x - a)\tan\Phi - y = 0 \tag{4}$$

The wire shadows were measured by rotating the X-ray beam around the g_φ axis for two values of the elevation angle, ϑ_1 and ϑ_2. The wire positions φ_1 and φ_2 were determined through a simple fitting procedure to a Gaussian plus a linear background. The measurement was repeated after rotating the BDD by 180^o around g_φ axis. From the measured profile centres of gravity φ_1,φ_2 (before rotation) and φ_1',φ_2' (after rotation), and the value of the distance d between the crossing point of the BDD axes and the wire plane, the wire line-parameters can be extracted from the following formulae:

$$\Phi = \arctan\left\{\frac{\tan\vartheta_2\sin\varphi_2^+ - \tan\vartheta_1\sin\varphi_1^+}{\tan\vartheta_2\cos\varphi_2^+ - \tan\vartheta_1\cos\varphi_1^+}\right\}, \tag{5}$$

$$a = d\frac{\tan\vartheta_1\tan\vartheta_2\sin(\varphi_2^+ - \varphi_1^+)}{\tan\vartheta_2\sin\varphi_2^+ - \tan\vartheta_1\sin\varphi_1^+}, \tag{6}$$

where

$$\varphi_i^+ = \frac{\varphi_i + \varphi_i'}{2}, \quad i = 1, 2 \quad .$$

The above formulae are valid in the linear approximation for small values of $\varepsilon_Y, \varepsilon_X$, α_G, ξ (as discussed in section 3) and for $\delta\varphi = \varphi_2 - \varphi_1 \ll 1$. It should be noted that, corrections to the wire positions, arising from possible non-coliniarity between the exit slit and the wire, are neglected in this procedure. There are two possible source for such a non-coliniarity : wire projection is not radial and the long component of the exit slit is not perpendicular to the g_ϑ axis. The corrections due to the latter source could not be neglected for these measurements. Therefore, the measurements of the wire positions were always repeated twice before and after rotation of the BDD by 180^o around the g_φ axis. The same procedure was used for the measurements of the wire positions in the TRT endcap wheel.

(in the direction perpendicular to the g_φ axis) under the control of a digital indicator, so as to minimise the values of ε_Y and α_G.

The wire shadows measured after adjustment are shown in Fig.12. The two measured positions of the wire placed close to the exit slit differ only by 2 μm. This sets an upper limit $\varepsilon_Y \leq 1\mu m$. The two measured positions of the second wire differ by 19 μm. Taking into account the distance between the two wires of $\sim$ 500 mm, an upper limit $\alpha_G \leq 3.5''$ (or $\sim$ 1.7 μrad) can be set.

4.2 X-ray beam adjustment in the vertical direction

A similar adjustment procedure is then applied for the vertical direction, as shown in Fig.13. An additional slit of about 1 mm width is placed between the NaI detector and the exit slit in two positions, i.e. close to the exit slit and at a distance of $\sim$ 500 mm. This slit was placed on a moveable support and its position was measured with an accuracy of $\sim$ 100 μm. The X-ray unit was then adjusted in the vertical direction to minimise the displacement ε_X. The profiles of the X-ray beam in the vertical direction for two positions of the BDD (before and after rotation by 180^o) are shown in Fig.14. This profile have a complicated structure, due to a significant non-uniformity of the X-ray beam intensity in this direction and to the less than ideal position of the first collimator placed after the X-ray tube. Nevertheless, these profiles display very sharp edges, which were used to adjust the vertical position of the X-ray beam. Fig.14 demonstrates that the differences between the positions of the beam profiles edges for the two positions of the BDD were reduced after adjustment to less than $2\varepsilon_X \leq 100\mu$m.

5 Calibration of the Beam Directing Device

To estimate the accuracy of the coordinate measurements by the BDD a special set of calibration measurements was performed. For this purpose, a special metallic wheel of $\sim$ 0.8 m diameter was constructed. This wheel contains eight slits in which tungsten wires of 50 μm diameter were installed (see Fig.15). The angle between these wires was approximately 45^o. The positions of the wires were measured with very high accuracy ($\sim$ 1 - 2 μm) by the metrology service and the angles between wires were calculated.

This wheel was placed at a distance of $\sim$ 300 mm from the exit slit of BDD. After adjustment of the X-ray beam relative to the calibration wheel, the shadow

b). for a given value of ϑ, the X-ray beam follows a circle, as the BDD is rotated around the g_φ axis (see Appendix B).

These correction have to be taken into account, in order to extract the wire positions from the BDD measurements.

4 X-ray beam adjustment

After the X-ray monochromator was installed into the BDD, a precise adjustment of the X-ray beam relatively to the BDD axis g_φ was performed in order to:

- minimise the displacement ε_Y to a value smaller than 10 μm in the direction perpendicular to the wires (horizontal); This corresponds to the narrow component of the exit slit, which has a size of $\sim$ 50 μm;
- minimise the displacement ε_X to a value below 100 μm in the direction along the wires (vertical), where the exit slit has a size of $\sim$ 22 mm;
- set the X-ray beam parallel to the Z axis, i.e. set $\alpha_G = 0$ with an accuracy better than $3''$.

4.1 X-ray beam adjustment in the horizontal direction

Fig.10 shows a sketch of the set-up for adjustment of the X-ray beam with respect to the g_φ (or Z) axis in horizon. In a first step, the BDD is placed on a rigid table, together with two tungsten wires of 50 μm diameter, serving as threads for a lead weight and placed in the path of the X-ray beam. The first of these wires is placed close to the exit slit and the second one at a distance of $\sim$ 500 mm. The wire supports are placed on a moveable table, which provides accurate movements of the wires over a short range of 1-2 mm. The wire positions are measured by a digital indicator with an accuracy of about 1 μm.

The X-ray beam profile is measured by observing the wire shadows in a NaI detector placed behind the wires. This profile measurement was repeated after rotating the X-ray beam around the g_φ axis by 180^o as illustrated in Fig.11. If the displacement ε_Y and the angle α_G are insignificant, the position of the wire shadows must coincide for the both positions of the BDD (before and after rotation). Using an adjustment screw, the X-ray unit was rotated and moved

and the measurement plane[4] perpendicular to the Z axis placed at a distance d from the centre of coordinates and the angles φ, ϑ measured by the BDD.

In general case, the X-ray beam direction are determined by five parameters, chosen as shown in Fig.9 :

- ε_Y - displacement in the horizontal direction;
- ε_X - displacement in the vertical direction;
- α_G - angle between X-ray beam and Z axis ;
- α_V - angle between X-ray beam and YZ plane ;
- l - z coordinate of the exit slit of the X-ray unit.

This parametrisation was chosen because all the above parameters could be directly measured in order to determine the X-ray beam position with the required accuracy. The value of the angle α_V can chosen to be 0, by simply redefining the rotation angle ϑ.

For the simplest case, when ε_Y,ε_X,α_G and ξ are equal to 0, this relationship is:

$$X = d \tan\vartheta \cos\varphi, \qquad Y = d \tan\vartheta \sin\varphi \tag{1}$$

In the case, where ε_Y,ε_X,α_G,ξ cannot be neglected, even after adjustment of the BDD, the relationship can be written as:

$$X = d \tan\vartheta \cos\varphi (1 - \xi \tan\varphi \frac{1-\cos\vartheta}{\sin\vartheta} + \frac{\varepsilon_X}{d \sin\vartheta} - \frac{\varepsilon_Y}{d} \tan\varphi \cot\vartheta - \alpha_G \tan\varphi \frac{d - l\cos\vartheta}{d \sin\vartheta}) \tag{2}$$

$$Y = d \tan\vartheta \sin\varphi (1 + \xi \cot\varphi \frac{1-\cos\vartheta}{\sin\vartheta} + \frac{\varepsilon_X}{d \sin\vartheta} + \frac{\varepsilon_Y}{d} \cot\varphi \cot\vartheta + \alpha_G \cot\varphi \frac{d - l\cos\vartheta}{d \sin\vartheta}), \tag{3}$$

where $\frac{\varepsilon_Y}{d}$, $\frac{\varepsilon_X}{d}$,ξ,$\alpha_G \ll 1$. Using the above equations it can be shown that :
a). for $\alpha_G \neq 0$ and $\xi \neq 0$ and a given value of φ, the X-ray beam follows a hyperbola instead of a straight line, as the BDD is rotated around the g_ϑ axis (see Appendix A);

[4]The position of the wires projection will be determined in this plane.

good agreement with the tabulated value 100:55 [5]. After this measurement the crystal was fixed to the angular position, which corresponds to the maximum intensity of the K_{α_1} line.

The characteristics of the outgoing X-ray beam after adjustment are summarised below:

- Energy : 36.03 keV (K_{α_1}Pr);
- Intensity : $\sim$ 8000 sec^{-1};
- Width at the exit slit : $\sim$ 50 μm;
- Height at the exit slit : $\sim$ 22 mm;
- Horizontal divergence : $\sim$ 50 μrad;
- Vertical divergence : $\sim$ 66 mrad;
- X-ray tube current : 25 μA;
- X-ray tube voltage : 90 kV.

3 Coordinate system of the BDD

As described in section 2, the Beam Directing Device (BDD) can rotate around two axes. The angular range used for rotations around the first axis g_φ (azimuthal angle φ) was the full range 360^o, range used around the second axis g_ϑ (elevation angle ϑ) was about $\pm$ 40^o.

Consider, that the axes g_φ and g_ϑ are crossing, but their crossing-angle may in reality slightly differ from a right angle by a small angle ξ. The value of this angle depends upon the manufacturing accuracy of the BDD axes.

Let us choose the following systems of coordinate for BDD (see Fig.9). The first global coordinate system is a motionless Cartesian (rectangular) coordinate system (XYZ), where $\overrightarrow{Z} = \overrightarrow{X} \times \overrightarrow{Y}$. The Z axis is identical to the rotation axis g_φ. The Y axis is chosen such that the rotation axis g_ϑ lies in the YZ plane. The centre of coordinates is placed at the crossing point between g_φ and g_ϑ axes. The measurements are usually quoted in this coordinate system.

An endcap wheel for the TRT can be represented as a set of planes perpendicular to the global Z-axis at a variable distance d from the centre of coordinates. Each plane contains N wires, and, in the ideal case, each wire i can be represented by a straight segment between its extremities at the innermost and outermost radii, corresponding to angles ϑ_{inner} and ϑ_{outer} and is characterised by its angle $\varphi = \frac{2\pi i}{N}$. The geometry of the BDD measurements is then determined by the relationship between the coordinates X,Y of the crossing point of X-ray beam

of the X-ray tube (1) and the monochromator. The electron beam (5) is focused by electrostatic (2) and magnetic (3) lenses onto a spot of about 40-50 μm in diameter. A thin praseodymium layer deposited on the inner surface of the beryllium exit window (6) is used as a target. The energy spectrum of the produced uncollimated X-ray beam is shown in Fig.6, and displays the usual bremsstrahlung spectrum with the characteristic lines for K_α and K_β emission of praseodymium.

The X-ray beam passing through a lead slit of 300 μm width (4) then impinges on the silicon crystal (7). The X-ray quanta with a wave-length satisfying the Bragg condition are diffracted from the silicon-crystal planes (111) and then pass through an exit slit (10) made of two tungsten cylinders (see Fig.5 also for details of the design). This exit slit has an adjustable width and can be rotated around the X-ray beam axis. The silicon crystal is clamped into the crystal-shaft (11) slot by a spring via a sliding block (9), which also serves as a jaw of the second collimating slit. The second jaw (8) of this collimating slit is placed after the crystal to intercept the direct non-diffracted X-ray beam. The crystal shaft can be rotated via a screw and lever (13) under the control of a dial (or digital) indicator, thus permitting to rotate the crystal into the Bragg position. The exit slit is fastened onto a lever (14) at a distance of ~ 200 mm from the crystal-shaft axis. The exit slit has to be set to the position corresponding to the double Bragg angle by rotating it around the crystal-shaft axis. This rotation is monitored by a second dial (or digital) indicator. The energy spectrum after the monochromator is shown on Fig.7. Only one peak corresponding to the K_{α_1} emission line of praseodymium remains in this spectrum after the monochromator. It should, however, be noted that there is a residual small bump at an energy of about 60 KeV. This background from the direct non-diffracted beam was subsequently suppressed by additional shielding of the exit slit.

Fig.8 shows the measured counting rate for the outgoing X-ray beam after the exit slit of the monochromator as a function of the angular position of the silicon crystal used for diffraction. To obtain this spectrum, for each angular position ϑ of the crystal, the exit slit is placed in the position corresponding to twice this angle ϑ, which is measured by the digital indicator in microns ($1\ \mu m \approx 1.8''$). The spectrum displays two peaks, corresponding to the K_{α_1} ($E_{K_{\alpha_1}} = 36.03\ KeV$) and K_{α_2} ($E_{K_{\alpha_2}} = 35.55\ KeV$) X-ray emission lines of praseodymium. The ratio between the intensities of the K_{α_1} line and of the diffraction background is about 7:1. The width (FWHM) of the K_{α_1} line is equal to $60''$ ($\sim 34\ \mu$m). The ratio between the intensities of K_{α_1} and K_{α_2} lines is measured to be 100:52 in

Inner Detector and for the simultaneous alignment of several wheels in the endcap TRT we have finally chosen a spherical geometry for the BDD.

Fig.1 shows photographs of the assembled BDD from two different sides and a schematic view is shown in Fig.2.

The BDD consists of two main parts : the X-ray apparatus with monochromator as a unit block (X-ray unit) and a device providing the possibility to direct the X-ray beam in a chosen direction within some solid angle.

The X-ray unit (1) is fixed to the frame by two opposed locking cones. This frame can rotate around the g_ϑ axis (see sect.3) through a stepping motor (2) via a double-reduction gear transmission[2] 1:72 (3). A high-precision Absolute Angle Encoder (4) (ROC 417, Heidenhain) is connected to the rotating shaft by an inflexible coupling. The shaft bearings are fastened to the frame (10) and connected rigidly to the shaft (5), which thus rotates around the horizontal axis on these two bearings installed on the support-frame. The chosen high-precision ball-bearings have a radial throbbing of less 1 μm. The angular rotations around the g_φ axis (see sec.3) are achieved through a second double-reduction gear transmission 1:648 (9) and a second stepping motor[3] (6). For the higher-accuracy angular measurements needed here, an Incremental Angle Encoder (IAE) with integral coupling (RON 905, Heidenhain) is used (7). This encoder is directly connected to the rotation axis. Thanks to this direct coupling between the angle encoder and the rotation axis there are no backlash effects, and the rotation of the apparatus is directly measured by the angle encoder. The backlash in the both gear transmissions is less than 1/10 of the angular measurement accuracy. The Incremental Angle Encoder provides a measurement of the rotation angle over the full range of 360^o with an accuracy not worse than of $0.2''$ per revolution. The measurement step of this encoder is approximately equal to $0.036''$ (with interpolation). The AAE has an accuracy of about $\pm 10''$ and a measurement step of $10''$. The BDD support-frame (8) has been built with adjustable legs in the vertical and horizontal directions.

The X-ray monochromator, as shown in Fig.3,4 and 5, consists of a High Voltage (HV) power supply (12) with the X-ray tube installed inside this HV block, a silicon crystal with its support, a collimator, an exit slit and a system allowing rotate of the crystal or the exit slit. Fig.3 shows a photograph of the X-ray monochromator installed inside its moveable frame. Fig.4 presents a sketch

[2]The stepping motor has an additional inner gear transmission ratio of 1:5, therefore one motor step is equal to $1.8''$

[3]one motor step is equal to $0.2''$

1 Introduction

A precise knowledge of the wire position inside the Straw Proportional Tubes (SPT), which are the basic building blocks of the ATLAS TRT, is an important physics requirement, which will contribute to minimise the errors in detecting and tracking high-energy particles deflected by the 2T solenoidal magnetic field within the ATLAS Inner Detector.

The overall mechanical tolerance on the individual SPT wire positioning has been set to $\pm$ 100 μm as decided in the May 1996 wheel review. An accurate tool for measuring a fraction of or all the wire positions after assembly is obviously needed, both to validate mechanical design and assembly procedures, and to ensure sufficient quality control during construction.

Some years ago, an X-ray diagnostic device for measuring accurately the SPT wire positions has been developed in PNPI [1,2]. Measurements on a small SPT prototype described in [2] have shown that the proposed X-ray calibration technique provides a reproducible high-accuracy measurements of the wire position to better than 10 μm. It was also shown that the achieved accuracy is not degraded if several wires overlap each other along the direction of the X-ray beam.

Taking into account these first measurements, we proposed to construct a measuring device providing the possibility to direct the X-ray beam in a chosen direction within some solid angle and supplying an accurate angle position measurement system [3]. This Beam Directing Device (BDD) was designed and assembled in PNPI.

In this note, we describe the design, the adjustment procedure and the calibration results of the BDD. Separate notes describe the results of the measurements performed in the full-scale endcap wheel prototype and the consequences for the final endcap design.

2 Design of the Beam Directing Device

Taking into consideration the SPT radial configuration in the endcap TRT as well as the X-ray beam profile (height: 22 mm, width: $\sim$ 50 μm), one concludes that a cylindrical or spherical coordinate system is preferable to a rectangular one for the BDD movement. The cylindrical geometry first considered in [2] seemed to be the most suitable one for the TRT wheel calibration although it is less universal than the spherical one proposed in [4]. In view of preserving the possibility to use this BDD for calibration of other subsystems of the ATLAS

Contents

ATLAS Internal Note
INDET-NO-161
1 March 1997

An X-Ray Measurement Station for the ATLAS Endcap TRT Calibration.

Part 1: Design, adjustment and testing.

V. Ivanov, O. Fedin, A. Jelamkov, S. Muraviev[1],
Yu. Platonov, A. Smirnov

PNPI, St.-Petersburg

Abstract

An X-ray Beam Directing Device (BDD) has been constructed to calibrate the ATLAS endcap Transition Radiation Tracker (TRT). The design of this BDD is described. The adjustment and calibration procedure is also discussed. Numerous examples to illustrate the BDD performance are presented. In particular, the results of the measurements of a special calibration wheel are described and compared to the metrology measurements. The results from the measurements of the full-scale endcap TRT wheel are presented in separate paper.

[1]Lebedev Physical Institute, Moscow